International Journal of Automotive Technology, Vol. 13, No. 2, pp. 255–261 (2012)
DOI 10.1007/s12239–012–0022–7

pISSN 1229–9138/ eISSN 1976–3832

NUMERICAL MODELING OF JOURNAL BEARING CONSIDERING BOTH ELASTOHYDRODYNAMIC LUBRICATION AND MULTI-FLEXIBLE-BODY DYNAMICS

J. CHOI[1)], S. S. KIM[2)], S. S. RHIM[3)] and J. H. CHOI[3)*]

[1)]Senior Research Engineer, FunctionBay, Inc., 5F Pangyo Seven Venture Valley 1 danji 2 dong, 625 Sampyeong-dong, Bundang-gu, Seongnam-si, Gyeonggi 463-400, Korea
[2)]School of Mechanical and Aerospace Engineering, Seoul National University, Seoul 151-742, Korea
[3)]Department of Mechanical Engineering, KyungHee University, Gyeonggi 446-701, Korea

(Received 8 November 2010; Revised 21 March 2011; Accepted 26 July 2011)

ABSTRACT–This study uses an elastohydrodynamic lubrication model coupled with multi-flexible-body dynamics (MFBD) to analyze dynamic bearing lubrication characteristics, such as pressure distribution and oil film thickness. To solve the coupled fluid-structure interaction system, this study uses an MFBD solver and an elastohydrodynamics module. The elastohydrodynamics module passes its force and torque data to the MFBD solver, which can solve general dynamic systems that include rigid and flexible bodies, joints, forces, and contact elements. The MFBD solver analyzes the positions, velocities, and accelerations of the multi-flexible-body system while incorporating the pressure distribution results of the elastohydrodynamics module. The MFBD solver then passes the position and velocity information back to the elastohydrodynamics solver, which reanalyzes the force, torque, and pressure distribution. This iteration is continued throughout the analysis time period. Other functions, such as mesh grid control and oil hole and groove effects, are also implemented. Numerical examples for bearing lubrication systems are demonstrated.

KEY WORDS : Journal bearing, Elastohydrodynamic lubrication, MFBD (Multi-Flexible-Body Dynamics), Fluid-structure interactions

1. INTRODUCTION

Journal bearings, which are the among the most widely used machine elements, transmit power while reducing friction and resisting external loads. In particular, in the common internal combustion engine, a variety of journal bearings are used between the piston, piston pin, connecting rod, crankshaft, and engine block. These journal bearings, which are under the alternating loads generated by the engine's combustion forces, guarantee the smooth operation of the engine and are important for the durability of the engine system. Recently, the realization of the importance of bearing lubrication analysis to achieving high-performance output and reducing engine weight has been increasing (Taylor 1993; Oh and Goenka, 1985; Labouff and Booker, 1985).

The study of bearing lubrication is based on the Reynolds equation (Reynolds, 1886), which describes the thickness and pressure of the fluid film generated by the relative motion of objects. In particular, Ott (1948) and Hahn (1957) first studied the relative motion of journal bearings, such as engine bearings resisting alternating loads. Dowson and Higginson (1959) developed numerical solutions for elastohydrodynamic problems. Hamrock and Dowson (1976) investigated oil film thickness and the relationships between contacts. To estimate lubrication film characteristics, such as the oil film thickness, pressure, power loss, and flow rate, an elastohydrodynamic lubrication analysis is needed. In addition, to calculate the relative displacements between the bearing and the journal, the theory of multi-flexible-body dynamics (MFBD) is needed (Peiskammer *et al*., 2002; Riener *et al*., 2001; Choi, 2009).

To obtain better results for lubrication characteristics, it is also important to consider the variation in the oil film thickness and the oil pressure resulting from the deformation of flexible bodies in the analysis of elastohydrodynamic lubrication. Thus, this paper proposes a model that includes these effects in the elastohydrodynamic lubrication analysis.

Generally, elastohydrodynamic lubrication can be classified into two types based on the relationship between surface roughness and oil film thickness. One type is full-film lubrication. It has been widely used when the lubricant film is sufficiently thick that there is no significant asperity contact. In this case, the pressure is only governed by the Reynolds equation, which was first established by Reynolds (1886). The other type of elastohydrodynamic lubrication is mixed lubrication. When the lubricant film is not thick,

**Corresponding author.* e-mail: jhchoi@khu.ac.kr

asperity contact between two bodies can occur (Zhu and Cheng, 1988; Greenwood and Tripp, 1971). Therefore, in a mixed lubrication region, the total pressure should be treated as the sum of the pressures induced by the fluid flow and the asperity contact.

In mixed lubrication regions, this paper uses the Reynolds equation to obtain the hydrodynamic pressure and Greenwood and Tripp's asperity contact model (1971) to obtain the asperity contact pressure. Oil hole and groove effects are included by applying pressure boundary conditions. Also, the dynamic viscosity of oil is modeled as a function of pressure using the Barus law (Dowson and Higginson, 1977).

In Section 2, the MFBD theory used in this study is introduced. The EHD governing equations are introduced in Section 3, and the analysis procedure for fluid-structure interactions is explained in Section 4. A numerical example is discussed in Section 5, and finally, the conclusions are presented in Section 6.

2. MULTI-FLEXIBLE-BODY DYNAMICS

In this section, brief formulations for MBD and MFBD are introduced. Detailed information is provided in Choi (2009).

2.1. MBD Formulation

The coordinate systems for two contiguous rigid bodies in 3D space are shown in Figure 1. Two rigid bodies are connected by a joint, and an external force, **F**, is acting on rigid body, *j*. The X-Y-Z frame is the global reference frame, and x′-y′-z′ is the body reference frame with respect to the X-Y-Z frame. The subscript *i* denotes the inboard body of body *j* in the spanning tree of a recursive formulation (Bae *et al*., 2001). In this section, the subscript *j* can be replaced with the subscript (*i*+1).

Velocities and virtual displacements of the origin of body reference frame x′-y′-z′ with respect to the global reference frame X-Y-Z are respectively defined as

$$\begin{bmatrix} \dot{\mathbf{r}} \\ \boldsymbol{\omega} \end{bmatrix} \tag{1}$$

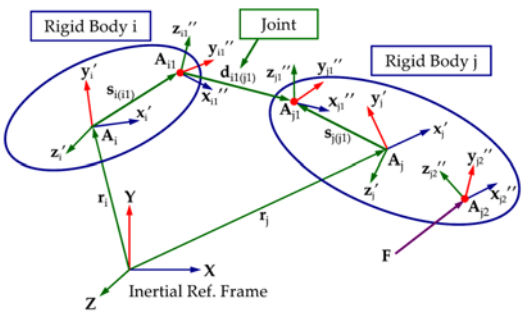

Figure 1. Two contiguous rigid bodies.

$$\begin{bmatrix} \delta\mathbf{r} \\ \delta\boldsymbol{\pi} \end{bmatrix} \tag{2}$$

Their corresponding quantities with respect to the body reference frame x′-y′-z′ are defined as

$$\mathbf{Y} = \begin{bmatrix} \dot{\mathbf{r}}' \\ \boldsymbol{\omega}' \end{bmatrix} \equiv \begin{bmatrix} \mathbf{A}^{\mathrm{T}}\dot{\mathbf{r}} \\ \mathbf{A}^{\mathrm{T}}\boldsymbol{\omega} \end{bmatrix} \tag{3}$$

$$\delta\boldsymbol{Z} = \begin{bmatrix} \delta\mathbf{r}' \\ \delta\boldsymbol{\pi}' \end{bmatrix} \equiv \begin{bmatrix} \mathbf{A}^{\mathrm{T}}\delta\mathbf{r} \\ \mathbf{A}^{\mathrm{T}}\delta\boldsymbol{\pi} \end{bmatrix} \tag{4}$$

where **A** is the orientation matrix of the x′-y′-z′ frame with respect to the X-Y-Z frame.

The recursive velocity equation for a pair of contiguous bodies is

$$\mathbf{Y}_j = \mathbf{B}_{ij}^1\mathbf{Y}_i + \mathbf{B}_{ij}^2\dot{\mathbf{q}}_{ij} \tag{5}$$

where **Y** is the combined velocity of the translation and rotation as defined in Equation (3), and $\mathbf{B}_{ij}^1$ and $\mathbf{B}_{ij}^2$ are defined as follows:

$$\mathbf{B}_{ij}^1 = \begin{bmatrix} \mathbf{A}_{ij}^{\mathrm{T}} & \mathbf{0} \\ \mathbf{0} & \mathbf{A}_{ij}^{\mathrm{T}} \end{bmatrix} \begin{bmatrix} \mathbf{I} & -(\tilde{\mathbf{s}}'_{ij} + \tilde{\mathbf{d}}'_{ij} - \mathbf{A}_{ij}\tilde{\mathbf{s}}'_{ji}\mathbf{A}_{ij}^{\mathrm{T}}) \\ \mathbf{0} & \mathbf{I} \end{bmatrix} \tag{6}$$

$$\mathbf{B}_{ij}^2 = \begin{bmatrix} \mathbf{A}_{ij}^{\mathrm{T}} & \mathbf{0} \\ \mathbf{0} & \mathbf{A}_{ij}^{\mathrm{T}} \end{bmatrix} \begin{bmatrix} \mathbf{I} & -(\mathbf{d}'_{ij})_{\mathbf{q}_{ij}} + \mathbf{A}_{ij}\tilde{\mathbf{s}}'_{ji}\mathbf{A}_{ij}^{\mathrm{T}}\mathbf{H}'_{ij} \\ \mathbf{0} & \mathbf{I} \end{bmatrix} \tag{7}$$

where $\mathbf{H}'_{ij}$ is determined by the axis of rotation (Bae *et al*., 2001; Choi, 2009). It is important to note that matrices $\mathbf{B}_{ij}^1$ and $\mathbf{B}_{ij}^2$ are only functions of $\mathbf{q}_{ij}$. Similarly, the recursive virtual displacement relationship is obtained as follows:

$$\delta\mathbf{Z}_j = \mathbf{B}_{ij}^1\delta\mathbf{Z}_i + \mathbf{B}_{ij}^2\delta\mathbf{q}_{ij} \tag{8}$$

If the recursive formula in Equation (5) is sequentially applied to all of the joints along the spanning tree, the following relationship between the Cartesian and relative generalized velocities can be obtained:

$$\mathbf{Y} = \mathbf{B}\dot{\mathbf{q}} \tag{9}$$

where **B** is the collection of coefficients of the $\dot{\mathbf{q}}_{ij}$ and

$$\mathbf{Y} = [\mathbf{Y}_0^{\mathrm{T}}, \mathbf{Y}_1^{\mathrm{T}}, \mathbf{Y}_2^{\mathrm{T}}, \ldots, \mathbf{Y}_n^{\mathrm{T}}]_{\mathrm{nc}}^{\mathrm{T}} \tag{10}$$

$$\dot{\mathbf{q}} = [\mathbf{Y}_0^{\mathrm{T}}, \dot{\mathbf{q}}_{01}^{\mathrm{T}}, \dot{\mathbf{q}}_{12}^{\mathrm{T}}, \ldots, \dot{\mathbf{q}}_{(n-1)n}^{\mathrm{T}}]_{\mathrm{nr}}^{\mathrm{T}} \tag{11}$$

where nc and nr denote the number of Cartesian and relative generalized coordinates, respectively. The Cartesian velocity $\mathbf{Y} \in \mathbf{R}^{\mathrm{nc}}$ with a given $\dot{\mathbf{q}} \in \mathbf{R}^{\mathrm{nr}}$ can be evaluated either by performing symbolic substitutions into Equation (9) or by using Equation (5) recursively with numerical substitution of the velocities $\mathbf{Y}_j$.

It is often necessary to transform vector $\mathbf{G}$ in $\mathbf{R}^{nc}$ into a new vector $\mathbf{g}=\mathbf{B}^{T}\mathbf{G}$ in $\mathbf{R}^{nr}$. This transformation is used, for example, when performing a generalized force computation in the joint space with a known force defined in the Cartesian space. The virtual work performed by the Cartesian force $\mathbf{Q}\in\mathbf{R}^{nc}$ is

$$\delta\mathbf{W}=\delta\mathbf{Z}^{T}\mathbf{Q} \tag{12}$$

where $\delta\mathbf{Z}$ must be kinematically admissible for all of the joints in a system. Substitution of $\delta\mathbf{Z}=\mathbf{B}\delta\mathbf{q}$ into Equation (12) yields

$$\delta\mathbf{W}=\delta\mathbf{q}^{T}\mathbf{B}^{T}\mathbf{Q}=\delta\mathbf{q}^{T}\mathbf{Q}^{*} \tag{13}$$

where $\mathbf{Q}^{*}\equiv\mathbf{B}^{T}\mathbf{Q}$.

The equations of motion for a constrained mechanical system (García de Jalón *et al*., 1986) in the joint space (Wittenburg, 1977) have been obtained by using the velocity transformation method as follows:

$$\mathbf{F}=\mathbf{B}^{T}(\mathbf{MY}+\Phi_{Z}^{T}\lambda-\mathbf{Q})=\mathbf{0} \tag{14}$$

where Φ and λ, respectively, denote the cut joint constraint and the corresponding Lagrange multiplier. $\mathbf{M}$ is the mass matrix, and $\mathbf{Q}$ is the force vector, which includes the external forces in the Cartesian space.

2.2. MFBD Formulation

The equations for the motion for the rigid body can be expanded from Equation (14) as follows:

$$\mathbf{F}^{r}=\mathbf{B}^{T}(\mathbf{MY}+\Phi_{z}^{rr\,T}\lambda^{rr}+\Phi_{z}^{er\,T}\lambda^{er}-\mathbf{Q}^{r})=\mathbf{0} \tag{15}$$

where the superscript *r* denotes a rigid body quantity, *rr* denotes a relative quantity between rigid bodies, and *er* represents a relative quantity between a flexible body node and a rigid body. A flexible body node is a node where flexion is permitted in a flexible body. The schematic diagram for two adjacent rigid and flexible bodies is shown in Figure 2.

The constraint equations between rigid bodies are expressed as a function of the rigid body generalized coordinates $\mathbf{q}^{r}$ as follows:

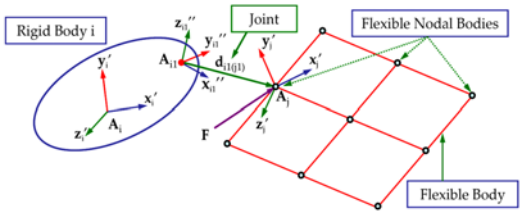

Figure 2. Two adjacent rigid and flexible bodies.

$$\Phi^{rr}=\Phi^{rr}(\mathbf{q}^{r},t) \tag{16}$$

Similarly, we can derive the equations of motion for the flexible body as follows:

$$\mathbf{F}^{e}=\mathbf{M}^{e}\ddot{\mathbf{q}}^{e}+\Phi_{\mathbf{q}^{e}}^{ee\,T}\lambda^{ee}+\Phi_{\mathbf{q}^{e}}^{er\,T}\lambda^{er}-\mathbf{Q}^{e}=0 \tag{17}$$

where $\mathbf{q}^{e}$ is the generalized coordinates for the flexible body nodes. The superscript *e* denotes a quantity describing a flexible body node, *ee* represents a relative quantity between flexible body nodes, and *er* denotes a relative quantity between a flexible body node and a rigid body. The forces $\mathbf{Q}^{e}$ between the flexible body nodes can be expressed as the sum of the element forces and applied forces, such as the gravity or contact forces, as follows:

$$\mathbf{Q}^{e}=\mathbf{Q}^{element}+\mathbf{Q}^{applied} \tag{18}$$

The flexible body joint constraints Φ^{er} between a flexible body node and a virtual rigid body can be expressed as follows:

$$\Phi^{er}=\Phi^{er}(\mathbf{q}^{e},\mathbf{q}^{r},t) \tag{19}$$

Similarly, the constraint equations Φ^{ee} between flexible body nodes can be expressed as in Equation (20).

$$\Phi^{ee}=\Phi^{ee}(\mathbf{q}^{e},t) \tag{20}$$

Finally, we can create the system matrix for the MFBD problem, as shown in Equation (21). We can solve Equation (21) using a sparse linear solver to find the incremental quantities, which are then added to the previous solution. This study used a generalized-alpha method for time integration (Chung and Hulbert, 1993).

$$\begin{bmatrix} \frac{\partial\mathbf{F}^{e}}{\partial\mathbf{q}^{e}} & \Phi_{\mathbf{q}^{e}}^{ee\,T} & \frac{\partial\mathbf{F}^{e}}{\partial\mathbf{q}^{r}} & \mathbf{0} & \Phi_{\mathbf{q}^{e}}^{er\,T} \\ \Phi_{\mathbf{q}^{e}}^{ee} & \mathbf{0} & \mathbf{0} & \mathbf{0} & \mathbf{0} \\ \frac{\partial\mathbf{F}^{r}}{\partial\mathbf{q}^{e}} & \mathbf{0} & \frac{\partial\mathbf{F}^{r}}{\partial\mathbf{q}^{r}} & \mathbf{B}^{T}\Phi_{z}^{rr\,T} & \mathbf{B}^{T}\Phi_{z}^{er\,T} \\ \mathbf{0} & \mathbf{0} & \Phi_{\mathbf{q}^{r}}^{rr} & \mathbf{0} & \mathbf{0} \\ \Phi_{\mathbf{q}^{e}}^{er} & \mathbf{0} & \Phi_{\mathbf{q}^{r}}^{er} & \mathbf{0} & \mathbf{0} \end{bmatrix} \begin{bmatrix} \Delta\mathbf{q}^{e} \\ \Delta\lambda^{ee} \\ \Delta\mathbf{q}^{r} \\ \Delta\lambda^{rr} \\ \Delta\lambda^{er} \end{bmatrix} = - \begin{bmatrix} \mathbf{F}^{e} \\ \Phi^{ee} \\ \mathbf{F}^{r} \\ \Phi^{rr} \\ \Phi^{er} \end{bmatrix} \tag{21}$$

3. ELASTOHYDRODYNAMICS (EHD)

3.1. Governing Equation of Hydrodynamics

Figure 3 shows a schematic diagram for the relative motion and dimensions of a bearing and a journal.

If we define R as the journal radius and C_r as the clearance in the journal bearing lubrication problem with laminar flow, the following assumptions can be made:

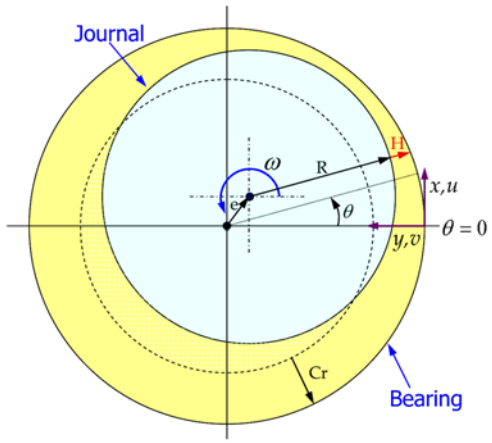

Figure 3. Schematic diagram of a journal bearing.

$$\left(\frac{C_r}{R}\right)^2 \ll 1$$
$$\mathrm{Re}\frac{C_r}{R} \ll 1 \left(Generally, \mathrm{Re}\frac{C_r}{R} \approx 0.001\right) \quad (22)$$

Under these assumptions, the governing equation for the fluid flow becomes the Couette-Poiseuille flow equation (Sabersky *et al*., 1989; Gohar, 2001; Jang *et al*., 2005). Then, if mass or flow rate conservation is applied, the Reynolds equation for the hydrodynamic problem can be expressed as follows:

$$\frac{\partial}{\partial x}\left(\Gamma\frac{\partial p}{\partial x}\right)+\frac{\partial}{\partial z}\left(\Gamma\frac{\partial p}{\partial x}\right)=12V+6U\frac{\partial H}{\partial x}+6W\frac{\partial H}{\partial z}$$
$$\Gamma=\frac{H^3}{\mu} \quad (23)$$

Here U, V, and W are the x, y, and z components of the relative velocity of the journal surface (at $y = H$), respectively, with respect to the bearing. H and μ are the oil film thickness and the dynamic (or absolute) viscosity, respectively. The discretization equation (Equation 23) is solved iteratively with the successive over-relaxation (SOR) method (Partankar, 1980).

In this study, the oil film thickness is defined as follows:

$$H(\theta) = C_r - e_x\cos\theta - e_y\sin\theta \quad (24)$$

As shown in Equation (23), the dynamic viscosity can vary spatially because it depends on the oil pressure. To account for the pressure-viscosity relation, this paper uses the Barus law (Dowson and Higginson, 1977):

$$\mu = \mu_0 e^{\alpha p} \quad (25)$$

Here, μ_0 is the dynamic viscosity in the atmospheric state, and α is the pressure-viscosity coefficient, which is related to the lubricant properties.

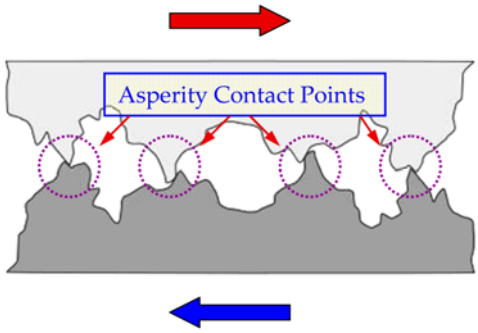

Figure 4. Example of asperity contact.

3.2. Asperity Contact Model

As shown in Figure 4, when the oil film is not thick compared to the surface roughness, the contact pressure resulting from the asperities between bodies should be considered.

In this paper, the asperity contact model of Greenwood and Tripp (1971) is used to model the mixed lubrication region. In Greenwood and Tripp's model, the asperity contact pressure p_a can be calculated as follows:

$$P_a(H) = KE'F_{5/2}(H/\sigma_s)$$
$$F_{5/2}(H/\sigma_s) = \begin{cases} 4.4086\times10^{-5}\left(4-\frac{H}{\sigma_s}\right)^{6.804}, & if\ \frac{H}{\sigma_s}<4 \\ 0, & otherwise \end{cases} \quad (26)$$

Here, K is the elastic factor, σ_s is the root mean square (rms) of the asperity summit heights, and E` is the composite elastic modulus, which is defined from the material properties of the contacting surfaces, as in Equation (27).

$$\frac{1}{E'} = \frac{1-\nu_1^2}{E_1}+\frac{1-\nu_2^2}{E_2} \quad (27)$$

Here, subscripts 1 and 2 denote the journal and bearing bodies, respectively. E is Young's modulus and ν is Poisson's ratio.

3.3. Compliance Effect

When a high external load is applied to a journal bearing, the oil pressure rapidly increases, and the oil film thickness is reduced. In this operating condition, it is necessary to include the elastic deformation of the bearing in the EHD model for better analysis of the lubrication characteristics because the deformation of the oil film can have important consequences for the pressure distribution and wear phenomena.

To incorporate the bearing deformation, this paper

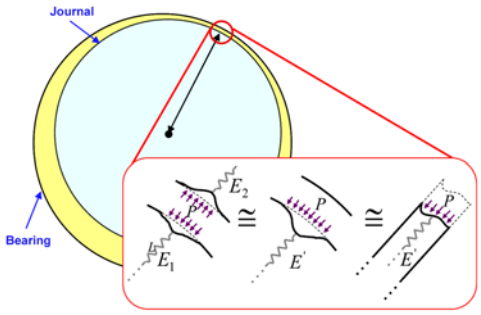

Figure 5. Equivalent model of surface deformation.

includes the elastic deformation effect in the analysis of dynamic bearing lubrication characteristics across a wide range of external loads. By quantifying the variation of the oil film thickness ΔH with the load and using the thickness value in the numerical procedure, we can analyze the effects of elastic deformation on the lubrication characteristics.

As shown in Figure 5, the sum of the elastic deformation of the surfaces of the journal and bearing is ΔH, where the Young's moduli of the journal and bearing are E_1 and E_2, respectively. This deformation is equivalent to the deformation solely of the surface of the journal with a Young's modulus E' that is a composite of E_1 and E_2 (Equation 27). In the equivalent model, ΔH is approximated as the variation in length of an object with Young's modulus E' and initial length L, where L is the journal radius when a normal pressure P is applied. Based on this approximation, the following equation is derived:

$$P \fallingdotseq E' \varepsilon \fallingdotseq E' \frac{\Delta H}{L} \tag{28}$$

The normal pressure P on the journal surface results from hydrodynamics and asperity contact. The following equation is the result:

$$\Delta H \fallingdotseq \frac{L}{E'} P \tag{29}$$

4. FLUID-STRUCTURE INTERACTIONS

In this study, as shown in Figure 6, EHD and MFBD solvers are used together to analyze the lubrication and multi-flexible-body dynamics of the journal bearing. First, pressure distributions are calculated in the hydrodynamic lubrication analysis. In this stage, the Reynolds equation (23) is solved with the asperity contact force (Equation 26) and the compliance effect (Equation 28) for the given boundary conditions, such as the positions and velocities of the bodies. Then, the calculated pressure field and the resulting forces and torques are passed to the MFBD solver. In the MFBD solver, the transferred pressure, force, and torque data are used as the external forces and torques acting on the journal and bearing bodies. In the MFBD analysis, the positions and velocities of all the bodies are

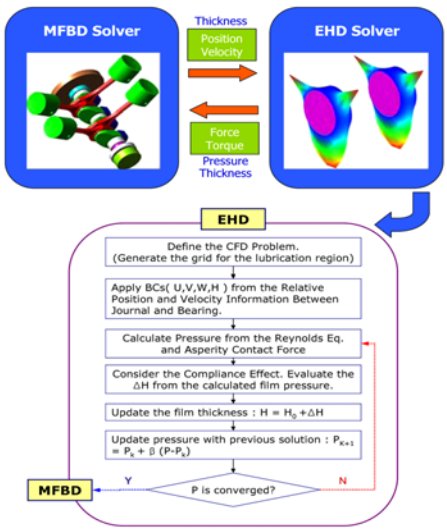

Figure 6. Fluid-structure interactions between the EHD and MFBD solvers.

calculated. From these position data, the center positions of the journal and bearing bodies are calculated, and the oil film thickness is evaluated over the EHD grid points. The journal and bearing radii are assumed to be constant. Finally, the oil film thickness and velocity at EHD grid points are transferred to the EHD solver as boundary conditions. The EHD and MFBD solvers are used iteratively to implement these procedures to analyze the lubrication and dynamic characteristics of the journal bearing.

To support a general-purpose EHD solution, groove and oil hole effects are implemented as pressure boundary conditions in the EHD solver.

5. NUMERICAL EXAMPLES

To implement the EHD module with the MFBD solver, this study used the RecurDyn™ (2010) MFBD environment.

To validate the numerical results of this study, the experimental results of Nakayama *et al*. (2003) were used. The numerical model has been described in detail in Nakayama *et al*. (2003). Figure 7 shows the numerical model and the measurement points of the oil film thickness. To measure the effect of the external load in the model, loads of 100 N, 200 N, 500 N, 1000 N, 1500 N, 2000 N, and 2500 N were applied. The rotational speed of the crankshaft was 3570 rpm.

Table 1 shows the simulation parameters used in the numerical model. Figure 8 shows the results for the pressure distribution according to the rotational angle for the grid points on the center circle. The pressure peak increases with increasing force, and the region of raised pressure is from about 50–180 deg, as expected. In Figure 9, the thickness results are compared with the experimental

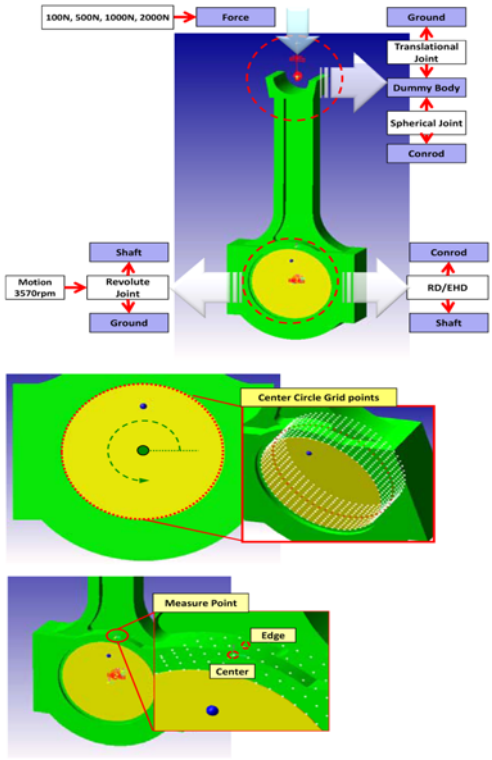

Figure 7. Numerical model for the journal bearing between the connecting rod and crankshaft.

Table 1. Parameters of the numerical model.

Parameters	Values
No. of grid (circum. × depth)	60×13
Journal diameter	45 mm
Bearing width	15.6 mm
Lubrication gap	0.068 mm
Dynamic viscosity	1.5e-2 Pa·s
Pressure-viscosity coeff.	1.28e-10 Pa^{-1}
Roughness	1.e-3 mm
Composite elastic modulus	57000 MPa
Elastic factor	3.e-3

results of Nakayama *et al*. (2003) at measured points to validate the model. As shown in Figure 9, the numerical results of the current study show good agreement with the experimental results.

6. CONCLUSION

In this study, elastohydrodynamic lubrication was coupled with multi-flexible-body dynamics (MFBD) to analyze dynamic bearing lubrication characteristics, such as

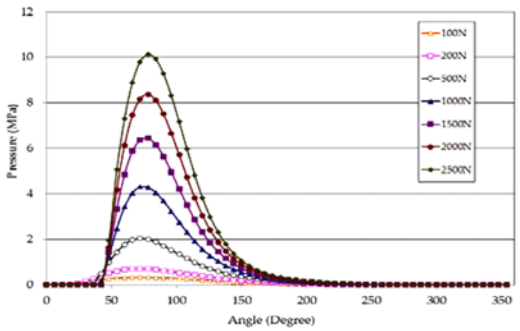

Figure 8. Numerical results for pressure distribution according to rotation angle for the grid points on the center circle.

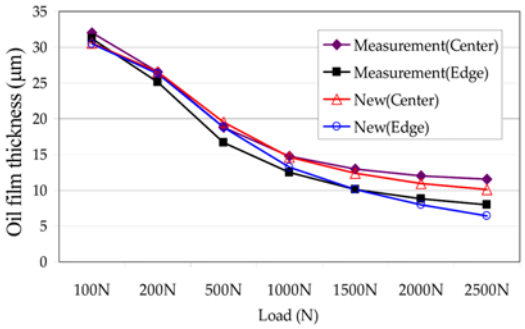

Figure 9. Comparison with measured results (Nakayama *et al*., 2003).

pressure distribution and oil film thickness. To solve the coupled fluid-structure interaction system, this study used an MFBD solver and an elastohydrodynamic module. The elastohydrodynamic lubrication module developed in this study transmits its pressure, force, and torque data to the MFBD solver, which can solve general dynamic systems. Then, the MFBD solver analyzes the positions and velocities of the multi-flexible-body system using the pressure, force, and torque results of the elastohydrodynamic module. The MFBD solver transmits the position and velocity data, from which the oil film thickness can be evaluated, to the EHD solver. Finally, the EHD solver calculates the oil pressure and the oil film thickness while accounting for compliance effects. These procedures are used iteratively between the MFBD and EHD solvers. Additionally, other functions, such as mesh grid control and oil hole and groove effects, were implemented. Finally, the numerical results were validated and compared with other experimental and numerical solutions using the journal bearing between the connecting rod and the crankshaft as an example.

REFERENCES

Bae, D. S., Han, J. M., Choi, J. H. and Yang, S. M. (2001). A

generalized recursive formulation for constrained flexible multibody dynamics. *Int. J. Numerical Methods in Engineering*, **50**, 1841–1859.

Choi, J. (2009). *A Study on the Analysis of Rigid and Flexible Body Dynamics with Contact.* Ph. D. Dissertation. Seoul Nat'l University. Seoul. Korea.

Chung, G. and Hulbert, G. M. (1993). A time integration algorithm for structural dynamics with improved numerical dissipation: Ther generalized-α method. *Trans. ASME*, *J. Applied Mechanics* **60**, **2**, 371–375.

Dowson, D. and Higginson, G. R. (1959). A numerical solution to the elastohydrodynamic problem. *J. Mech. Eng. Sci.*, **1**, 6–15.

Dowson, D. and Higginson, G. R. (1977). *Elastohydrodynamic Lubrication.* SI Edn. Chapter 6. Pergamon Press. Oxford.

García de Jalón, D. J., Unda, J. and Avello, A. (1986). Natural coordinates for the computer analysis of multibody systems. *Computer Methods in Applied Mechanics and Engineering*, **56**, 309–327.

Gohar, R. (2001). *Elastohydrodynamics.* 2nd Edn. Imperial College Press. London.

Greenwood, J. A. and Tripp, J. H. (1971). The contact of two nominally flat rough surfaces. *Proc. Instn. Mech. Engrs.*, Part 1, **185**, **48**, 625–633.

Hahn, H. W. (1957). Das Zulindrische Gleitlager endlicher Breite unter zeitlich veranderlicher Belastung. *Diss. TH. Karlsruhe*. Germany.

Hamrock, B. J. and Dowson, D. (1976). Isothermal elastohydrodynamic lubrication of point contacts, Part I, Theoretical Formulation. *ASME J. Lubr. Technol.*, **98**, 223–229.

Labouff, G. A. and Booker, J. F. (1985). Dynamically loaded journal bearings: A finite element treatment for rigid and elastic surfaces. *ASME*, *J. Tribology* **107**, **4**, 505–515.

Nakayama, K., Morio, I., Katagiri, T. and Okamoto, Y. (2003). A study for measurement of oil film thickness on engine bearing by using laser induced fluorescence (LIF) method. *SAE Int.*

Oh, K. P. and Goenka, P. K. (1985). The elastohydrodynamic solution of journal bearings under dynamic loading. *ASME*, *J. Tribology* **107**, **3**, 389–395.

Ott, H. H. (1948). *Zylindrische Gleitlager unter instationarer Belastung*. Diss. ETH. Zurich.

Patankar, S. V. (1980). *Numerical Heat Transfer and Fluid Flow*. Hemisphere. Washington.

Peiskammer, D., Riener, H., Prandstotter, M. and Steinbatz, M. (2002). Simulation of motor components : Intergration of EHD - MBS - FE – Fatigue. *ADAMS User Conf.*.

RecurDyn™ Manual (2010). http://www.functionbay.co.kr, FunctionBay, Inc..

Reynolds, O. (1986). On the theory of lubrication and its application to Mr. Beauchamp tower's experiments, including an experimental determination of the viscosity of olive oil. *Phil. Trans. Roy. Soc.*, **177**, 157–234.

Riener, H., Prandstotter, M. and Witteveen, W. (2001). Conrod Simulation: Integration on EHD - MBS - FE – Fatigue. *ADAMS User Conf.*.

Sabersky, R. H., Acosta, A. J. and Hauptmann, E. G. (1989). *Fluid Flow: A First Course in Fluid Mechanics.* 3rd Edn. Maxwell Macmillan Int. Edn. New York.

Jang, S. and Park, Y. (2005). Study on the effect of aerated lubricant on the journal trace in the engine bearing clearance. *Int. J. Automotive Technology* **6**, **4**, 421–427.

Taylor, C. M. (1993). *Engine Tribology.* Elsevier. Netherlands. 75–87.

Wittenburg, J. (1977). *Dynamics of Systems of Rigid Bodies.* B. G. Teubner. Stuttgart.

Zhu, D. and Cheng, H. S. (1998). Effect of surface roughness on the point contact EHL. *Trans. ASME*, *J. Tribology*, **110**, 32–37.